

Electrical Signature of the Percolation Threshold in Sea Ice

K. M. Golden¹, H. Eicken², A. Gully¹, M. Ingham³, K. A. Jones³, J. Lin¹, J.
E. Reid⁴, C. S. Sampson¹, and A. P. Worby⁵

Corresponding author: K. M. Golden, University of Utah, Department of Mathematics, 155 S
1400 E, RM 233, Salt Lake City, UT 84112-0090, USA. (golden@math.utah.edu)

3 Fluid flow through sea ice governs a broad range of geophysical and bi-
 4 ological processes in the polar marine environment. For example, the evo-
 5 lution of melt ponds and sea ice albedo, which is important in climate mod-
 6 eling, is constrained by drainage through the porous brine microstructure.
 7 However, for brine volume fractions below about 5%, columnar sea ice is ef-
 8 fectively impermeable to fluid flow. In two different experiments conducted
 9 in the Arctic and Antarctic, we have found that this critical fluid transition

¹University of Utah, Department of
 Mathematics, 155 S 1400 E, RM 233, Salt
 Lake City, UT 84112-0090, USA.
 (golden@math.utah.edu)

²University of Alaska Fairbanks,
 Fairbanks, AK, 99775-7320, USA.

³School of Chemical and Physical
 Sciences, Victoria University of
 Wellington, P.O. Box 600, Wellington, NZ.

⁴Groundprobe Geophysics, 1/288 Victoria
 Rd., Malaga 6090, AU.

⁵Australian Antarctic Division and ACE
 CRC, University of Tasmania, Private Bag
 80, Hobart, 7001, AU.

10 exhibits a strong electrical signature, with sea ice resistivity rising sharply
11 over three orders of magnitude near the brine connectivity threshold. The
12 data are accurately explained by percolation theory, with the same univer-
13 sal critical exponent which captures fluid permeability. These results enable
14 us to connect specific electrical profiles to important transport processes such
15 as melt pond drainage, CO₂ pumping, and the flux of nutrients which sus-
16 tain biomass build-up.

Key Points:

1. Data on the electrical resistivity of sea ice were taken in the Arctic and Antarctic
2. A strong electrical response near the brine percolation threshold is observed and explained theoretically
3. The results enable remote monitoring of key sea ice processes and transitions

1. Introduction

Polar sea ice is a key component of Earth's climate system, and a leading indicator of climate change [Thomas and Dieckmann, 2009; Serreze *et al.*, 2007]. As a material sea ice is a composite of pure ice with brine and air inclusions. The brine phase hosts extensive microbial communities which sustain life in the polar oceans [Thomas and Dieckmann, 2009; Fritsen *et al.*, 1994]. Fluid flow through the porous microstructure mediates key processes impacting the climatology and biology of sea ice. Improving projections of the fate of Earth's sea ice cover and its ecosystems depends on a better understanding of these important processes and feedback mechanisms.

For example, the evolution of sea ice albedo represents a fundamental problem in climate modeling and a significant source of uncertainty in climate projections [Flocco *et al.*, 2010; Polashenski *et al.*, 2012]. The albedo of sea ice floes is determined by melt pond evolution [Perovich *et al.*, 2002; Polashenski *et al.*, 2012]. Drainage of the ponds, with a resulting increase in albedo, is largely controlled by the fluid permeability of the porous sea ice underlying the ponds [Eicken *et al.*, 2004; Golden *et al.*, 2007]. As ice recedes with melting, more water surface is exposed, which increases solar absorption, leading in turn

to more melting, and so on. This *ice-albedo feedback* has played a significant role in the decline of the summer Arctic ice pack [Perovich et al., 2007].

Fluid flow through sea ice governs the evolution of the salt budget and salinity profiles [Thomas and Dieckmann, 2009], convection-enhanced thermal transport [Lytle and Ackley, 1996], ocean-ice-atmosphere CO₂ exchanges [Rysgaard et al., 2009], and the build-up of algal biomass fueled by nutrient fluxes [Thomas and Dieckmann, 2009; Fritsen et al., 1994]. It also drives snow-ice formation, accounting for a significant portion of the ice produced in the Southern Ocean [Maksym and Markus, 2008]. Sea water percolates upward through the porous microstructure, flooding the snow layer, and subsequently freezing.

While fluid flow is substantially restricted for brine volume fractions ϕ below about 5%, columnar sea ice is increasingly permeable for ϕ above 5% [Golden et al., 1998]. For a typical bulk salinity of 5 ppt, the critical porosity $\phi_c \approx 5\%$ corresponds to a temperature $T_c \approx -5^\circ$ C. This critical behavior of the fluid permeability, which is known as the *rule of fives*, results from a connectivity or percolation threshold in the brine microstructure [Golden et al., 1998, 2007; Pringle et al., 2009].

If the fluid transport properties of sea ice can be linked to its electrical properties, which is the aim of this paper, then new approaches can be brought to bear in monitoring the state of sea ice. For example, it could open the door to the development of sensors to enhance existing buoy networks, provide information on key ice processes, and improve integration with satellite data.

The electrical conductivity of sea ice has been studied over the past five decades [Fujino and Suzuki, 1963; Addison, 1969; Thyssen et al., 1974; Buckley et al., 1986; Reid et al.,

2006; *Ingham et al.*, 2008]. However, there have been no observations of critical behavior in electrical properties corresponding to the microstructural transition encapsulated in the rule of fives. Here we report on two types of experiments where electrical resistivity data clearly display critical behavior at the brine percolation threshold. The mathematical description we develop provides a rigorous link between fluid and electrical transport in sea ice, with both displaying the same type of universal critical behavior, thus laying the foundation for the techniques referred to above. In fact, we further develop this foundation by partitioning the range of resistivity values of our data into intervals which correspond to distinct regimes of fluid permeability characteristics and related process behavior, such as melt pond development, and fluxes of nutrients and CO₂.

One of the goals of this work is to obtain data on the linkages between electrical and hydraulic properties [*Wong*, 1988]. The value of such an approach lies in the potential to then extract information about other key variables describing the state of sea ice, e.g., pertaining to its rheology or potential to harbor microbial communities. Our results indicate that such information could potentially be obtained from measurements of electric properties via *in situ* drifting sensors that can monitor the evolution of sea ice non-destructively (Figure 1 d).

The findings presented here also have implications for measuring ice thickness, an important gauge of the impact of global warming. Not only is thickness data important in comparing climate model predictions to observed behavior, but in specifying the initial conditions necessary for long-term numerical simulations. Promising techniques for advanced airborne or surface-based measurements of ice thickness depend on the interaction

of electromagnetic (EM) fields with sea ice. For example, there has been significant interest in the development of EM induction devices [Haas, 2004; Reid *et al.*, 2006] mounted on ships, planes and helicopters. These techniques, and the interpretation of the data to obtain thickness information, rely on knowledge of the electrical properties of sea ice, and how they vary with depth, temperature, salinity, and ice type. The results presented here shed significant light on such issues.

2. Measuring the electrical properties of sea ice

Sea ice is an anisotropic composite with vertically elongated brine inclusions and corresponding anisotropy in the effective fluid permeability and electrical conductivity tensors. Most methods for measuring sea ice conductivity involve indirect or inverse techniques, such as surface-based geoelectric profiling using a Wenner array of electrodes [Fujino and Suzuki, 1963; Thyssen *et al.*, 1974; Buckley *et al.*, 1986; Reid *et al.*, 2006; Ingham *et al.*, 2008; Sampson *et al.*, 2011]. Generally with these methods the vertical conductivity σ_v^* is inherently mixed with the horizontal components. Here we are most interested in σ_v^* due to its connection with vertical fluid flow.

During the Sea Ice Physics and Ecosystem Experiment (SIPEX) in September and October of 2007, we made *direct* measurements of σ_v^* in Antarctic pack ice by adapting a four probe Wenner array for use in cylindrical ice cores, as shown in Figure 1 a and b. The study area was located off the coast of East Antarctica, between 115° E and 130° E, and 64° S and 66° S. At 8 of the 15 ice stations along the cruise track of the Australian icebreaker *Aurora Australis*, we extracted vertical cores from thin first-year sea ice, with lengths ranging from 34 cm to 86 cm. Thermistor probes were inserted into small holes

drilled every 5 cm. We used a Wenner electrode array along sections of the cores, connected to a YEW Earth Resistance Tester operating at 38 Hz. This set-up yields the resistance along the axis of the cylindrical ice core between probes P1 and P2, corresponding to the vertical direction *in situ*, with $a = L = 10$ cm (or $a = L = 5$ cm in some cases). We obtained 26 averaged data points from 67 raw measurements of the resistance between the inner probes. After the temperature and resistance measurements were taken, which took about 10 to 20 minutes, we cut each core into 10 cm sections which were later melted, so that we could obtain bulk salinity measurements for each section. The temperature and salinity measurements allowed us to calculate a brine volume fraction profile for each core [Eicken, 2003]. In the auxiliary material we demonstrate that the Wenner array deployed along the core axis is a viable field method for measuring conductivity, yielding values of the vertical component very close to the results of classical, parallel plate experiments.

In the Arctic, we used the technique of cross-borehole DC resistivity tomography [Ingham *et al.*, 2008; Jones *et al.*, 2010], as shown in Figure 1 c and d. The ice is probed in its natural state, utilizing two or four vertical strings of electrodes frozen into the ice. It has been shown that this method can be used to derive the horizontal component of the anisotropic resistivity profile. Moreover, it has been demonstrated that the vertical component of σ^* can be obtained as well [Jones *et al.*, 2010; Ingham *et al.*, 2008]. If a minimum of four electrode strings are used, the geometric mean of the vertical and horizontal components of σ^* can be derived, along with the horizontal component [Ingham *et al.*, 2008], yielding the vertical component.

Measurements of the temporal variation in the resistivity structure of first-year Arctic sea ice through spring warming have been made approximately 1 km off the coast of Barrow, Alaska at $71^{\circ} 21' 56.45''$ N, $156^{\circ} 32' 39.01''$ W. Electrode strings were installed in landfast first year ice in late January 2008. Cross-borehole measurements were made on 6 separate occasions between early April and mid June 2008, allowing both the horizontal and vertical components of the ice resistivity to be derived. A sea ice mass balance site and an ice core sampling program at the same location [Druckenmiller *et al.*, 2009] provided ice temperature and salinity data, allowing the variation in resistivity structure to be correlated with brine volume fraction ϕ .

3. Modeling the electrical conductivity of sea ice

Lattice and continuum percolation models [Stauffer and Aharony, 1992] have been used to study a broad range of disordered materials where the connectedness of one phase dominates effective transport behavior. In sea ice, the fluid and electrical transport properties are largely determined by the connectedness of the brine phase – an electrically conducting fluid. Here we briefly describe a lattice percolation model which provides the theoretical framework for predicting the electrical conductivity of sea ice, as well as its fluid permeability. This model, and how it is adapted to the microstructure of sea ice, is covered in more detail in the auxiliary material.

Consider the two dimensional square network of bonds (edges) joining nearest neighbor sites (vertices) in the integer lattice \mathbb{Z}^2 , as shown in Figure 2 a and b. The bonds are assigned electrical conductivities $\sigma_0 > 0$ (open) or 0 (closed) with probabilities p and $1 - p$, so that a relative proportion p of the bonds are open (on average). The *percolation*

threshold p_c is the smallest value of p for which an infinite, connected cluster of open bonds forms. In two dimensions ($d = 2$), $p_c = \frac{1}{2}$, and in three ($d = 3$), $p_c \approx 0.25$. For p just above the percolation threshold, $p > p_c$, where conducting pathways span the infinite lattice, the effective or bulk conductivity $\sigma^*(p)$ takes off with power law behavior,

$$\sigma^*(p) \sim \sigma_0(p - p_c)^t, \quad (1)$$

where t is the conductivity critical exponent. For lattices, t is believed to be universal, depending only on dimension and not, for example, on whether the lattice is square or triangular. In $d = 2$, $t \approx 1.3$, and in $d = 3$, $t \approx 2.0$ [Stauffer and Aharony, 1992].

In applying percolation theory to sea ice, it is useful to consider the vertical conductivity formation factor $F = \sigma_v^*/\sigma_b$, which removes the dependence of the effective parameter on the changing conductivity σ_b of the brine. In view of (1),

$$F(\phi) \sim F_0 (\phi - \phi_c)^2, \quad (2)$$

where $\phi_c \approx 0.05$ [Golden et al., 1998, 2007; Pringle et al., 2009], and $t \approx 2.0$, the $d = 3$ universal lattice value. Even though sea ice is a continuum, its lognormally distributed pores lead to universal critical behavior [Golden et al., 2007; Berkowitz and Balberg, 1992].

The scaling factor F_0 is obtained by relating the electrical conductivity to the fluid permeability of sea ice obtained in [Golden et al., 2007], through a critical (or *bottleneck*) radius r_c [Friedman and Seaton, 1998]. By measuring the radii of vertical pathways in X-ray tomography images [Golden et al., 2007; Pringle et al., 2009], we estimate a range in mm of $0.1 \leq r_c \leq 0.2$, yielding a range for F_0 of $6 \leq F_0 \leq 24$. These relations between fluid and electrical transport in sea ice are developed in the auxiliary material.

4. Comparison of theory and data

In order to compare our conductivity measurements with percolation theory, we must exclude data below $\phi_c \approx 0.05$ [Golden *et al.*, 2007], since the theory is only valid for $\phi > \phi_c$. It is more illustrative to display the data in terms of the reciprocal $G = 1/F = \rho_v^*/\rho_b$, which is the vertical resistivity formation factor. As the conductivity F becomes very small near ϕ_c , its reciprocal G becomes very large, with its behavior approximating a vertical asymptote near $\phi = \phi_c$. In Figure 2 c and d we show the two data sets from the Antarctic and Arctic. By fixing the exponent $t = 2$ and the threshold value $\phi_c = 0.05$ in the above expression for $F(\phi)$, a statistical best fit of the data yields a value of $F_0 \approx 9$, which lies inside our predicted range, so that $F(\phi) \sim 9 (\phi - 0.05)^2$.

We see that the data agree well with the theory, and that they both exhibit divergent behavior with a vertical asymptote at the percolation threshold. Moreover, in the variables $x = \log(\phi - 0.05)$ and $y = \log F$, the line predicted by percolation theory is $y = 2x + \log F_0$, with $\log F_0 = 0.95$, $F_0 = 9$. Critical path analysis yields the bounds $0.8 \leq \log F_0 \leq 1.4$, and the best fit for the Antarctic data in f is $y = 1.99x + 0.93$, where 0.93 lies inside these bounds. In logarithmic variables, the error of the regression is 0.38 for the Arctic data and 0.22 for the Antarctic data (that is, approximately 68% of the Antarctic data is within 0.22 of the regression line). The increased scatter in the Arctic data is not surprising given the inverse computation required.

To model $\sigma_v^*(\phi)$ over all porosities, we consider features of the brine phase present over the full range — some degree of small-scale connectivity, and self-similarity. Hierarchical models of spheres or other grains surrounded by smaller spheres, and so on, with brine

in the pore spaces [*Golden et al.*, 2007], were used to model $k_v^*(\phi)$. The simplest model yields a result of $k_v^*(\phi) = k_0 \phi^3$ and an Archie’s law $F(\phi) = F_0 \phi^3$. A statistical best fit of our Antarctic data yields a value of $F_0 \approx 16$, which is in the estimated range. In Figure 3 a, our Antarctic data is shown along with fits derived from both models, and in b, Arctic permeability data [*Golden et al.*, 2007] is shown relative to predictions from both models.

5. Discussion

Figure 4 illustrates how we can derive information about the permeability structure and relevant transport processes from resistivity soundings of Arctic sea ice with *in situ* electrode strings [*Jones et al.*, 2010]. Thus, the different formation factor regimes shown correspond to different permeability classes, with the lowermost ice layers permeable enough to allow for gas and nutrient exchange conducive to biomass build-up and CO₂ pumping [*Rysgaard et al.*, 2007], based on a critical permeability of 4×10^{-11} m², corresponding to a resistivity formation factor of 31.3 for $r_c = 0.1$ mm. This permeable base layer increases in vertical extent as the ice warms and thins due to bottom and surface melt. The ice interior is permeable enough to allow for meltwater flushing and reduction of ice salinity at surface ablation rates of 10 cm/d or less even prior to the onset of melt [*Freitag and Eicken*, 2003], corresponding to a resistivity formation factor of 625. High resistivity formation factors near the top in Figure 4 b are in part explained by such percolation of freshwater below accumulations of surface melt water.

6. Conclusions

It has been demonstrated in field experiments conducted in both the Arctic and Antarctic that sea ice exhibits critical behavior in its electrical transport properties at a per-

colation threshold. Such behavior provides the electrical signature of a key transition in fluid transport properties, known as the *rule of fives*, which determines whether or not fluid can flow through sea ice. This transition constrains a broad range of processes which are important in the geophysics and biology of the polar regions. The phenomenon is explained theoretically using percolation theory, which provides a universal power law describing the data from both poles, as well as a rigorous link between the fluid and electrical transport properties of sea ice. Our findings open the door to a new generation of techniques for *in situ* analysis and remote monitoring of transport processes, which can improve projections of the fate of Earth's ice packs and the response of polar ecosystems.

Acknowledgments. We are grateful for the support provided by the Division of Mathematical Sciences (DMS), the Arctic Natural Sciences (ARC) Program, and the Office of Polar Programs (OPP) at the US National Science Foundation (NSF) through grants DMS-0537015, DMS-0940249, and ARC-0934721. Joyce Lin was supported by an NSF Postdoctoral Fellowship through a VIGRE grant (DMS-0602219) to the Department of Mathematics at the University of Utah. Adam Gully and Christian Sampson were partially supported by the NSF Research Experiences for Undergraduates (REU) Program through the VIGRE grant, and graduate support through VIGRE. This work was also supported in part by the Australian Government through the Antarctic Climate and Ecosystems Cooperative Research Centre. Finally, we thank the crew of the *Aurora Australis* for their help and support during the SIPEX Antarctic expedition.

References

Addison, J. (1969), Electrical properties of saline ice, *J. Appl. Phys.*, *40*, 3105–3114.

- 214 Berkowitz, B., and I. Balberg (1992), Percolation approach to the problem of hydraulic
215 conductivity in porous media, *Transport in Porous Media*, 9, 275–286.
- 216 Buckley, R. G., M. P. Staines, and W. H. Robinson (1986), In situ measurements of the
217 resistivity of Antarctic sea ice, *Cold Reg. Sci. Technol.*, 12(3), 285–290.
- 218 Druckenmiller, M. L., H. Eicken, M. A. Johnson, D. J. Pringle, and C. C. Williams (2009),
219 Towards an integrated coastal sea-ice observatory: System components and a case study
220 at Barrow, Alaska, *Cold Reg. Sci. Technol.*, 56, 61–72.
- 221 Eicken, H. (2003), Growth, microstructure and properties of sea ice, in *Sea Ice: An*
222 *Introduction to its Physics, Chemistry, Biology and Geology*, edited by D. N. Thomas
223 and G. S. Dieckmann, pp. 22–81, Blackwell, Oxford.
- 224 Eicken, H., T. C. Grenfell, D. K. Perovich, J. A. Richter-Menge, and K. Frey (2004), Hy-
225 draulic controls of summer Arctic pack ice albedo, *J. Geophys. Res. (Oceans)*, 109(C18),
226 C08,007.1–C08,007.12, doi:10.1029/2003JC001989.
- 227 Flocco, D., D. L. Feltham, and A. K. Turner (2010), Incorporation of a physically based
228 melt pond scheme into the sea ice component of a climate model, *J. Geophys. Res.*, 115,
229 C08,012 (14 pp.), doi:10.1029/2009JC005,568.
- 230 Freitag, J., and H. Eicken (2003), Meltwater circulation and permeability of Arctic summer
231 sea ice derived from hydrological field experiments, *J. Glaciol.*, 49, 349–358.
- 232 Friedman, A. P., and N. A. Seaton (1998), Critical path analysis of the relationship
233 between permeability and electrical conductivity of three-dimensional pore networks,
234 *Water Resources Res.*, 34(7), 1703–1710.

- 235 Fritsen, C. H., V. I. Lytle, S. F. Ackley, and C. W. Sullivan (1994), Autumn bloom of
236 Antarctic pack-ice algae, *Science*, *266*, 782–784.
- 237 Fujino, K., and Y. Suzuki (1963), An attempt to estimate the thickness of sea ice by
238 electrical resistivity method ii, *Low Temp. Sci.*, *A21*, 151–157.
- 239 Golden, K. (1990), Convexity and exponent inequalities for conduction near percolation,
240 *Phys. Rev. Lett.*, *65*(24), 2923–2926.
- 241 Golden, K. M., S. F. Ackley, and V. I. Lytle (1998), The percolation phase transition in
242 sea ice, *Science*, *282*, 2238–2241.
- 243 Golden, K. M., H. Eicken, A. L. Heaton, J. Miner, D. Pringle, and J. Zhu (2007), Thermal
244 evolution of permeability and microstructure in sea ice, *Geophys. Res. Lett.*, *34*, L16,501
245 (6 pages and issue cover), doi:10.1029/2007GL030,447.
- 246 Haas, C. (2004), Late-summer sea ice thickness variability in the Arctic Transpolar Drift
247 1991-2001 derived from ground-based electromagnetic sounding, *Geophys. Res. Lett.*,
248 *31*, L09,402, doi:10.1029/2007GL030,447.
- 249 Halperin, B. I., S. Feng, and P. N. Sen (1985), Differences between lattice and continuum
250 percolation transport exponents, *Phys. Rev. Lett.*, *54*(22), 2391–2394.
- 251 Ingham, M., D. J. Pringle, and H. Eicken (2008), Cross-borehole resistivity tomography
252 of sea ice, *Cold Reg. Sci. Technol.*, *52*, 263–277, 10.1016/j.coldregions.2007.05.002.
- 253 Jones, K. A., M. Ingham, D. J. Pringle, and H. Eicken (2010), Temporal variations in sea
254 ice resistivity: resolving anisotropic microstructure through cross-borehole dc resistivity
255 tomography, *J. Geophys. Res.*, *115*, C11,023, doi:10.1029/2009JC006,049.

Lytle, V. I., and S. F. Ackley (1996), Heat flux through sea ice in the Western Weddell Sea:

Convective and conductive transfer processes, *J. Geophys. Res.*, *101*(C4), 8853–8868.

Maksym, T., and T. Markus (2008), Antarctic sea ice thickness and snow-to-ice conversion

from atmospheric reanalysis and passive microwave snow depth, *J. Geophys. Res.*, *113*,

C02S12, doi:10.1029/2006JC004,085.

Perovich, D. K., T. C. Grenfell, B. Light, and P. V. Hobbs (2002), Seasonal evolution

of the albedo of multiyear Arctic sea ice, *J. Geophys. Res. (Oceans)*, *107*(C10), 8044,

doi:10.1029/2000JC000,438.

Perovich, D. K., B. Light, H. Eicken, K. F. Jones, K. Runciman, and S. V. Nghiem

(2007), Increasing solar heating of the Arctic Ocean and adjacent seas, 1979-2005:

Attribution and role in the ice-albedo feedback, *Geophys. Res. Lett.*, *34*, L19,505,

doi:10.1029/2007GL031,480.

Polashenski, C., D. Perovich, and Z. Courville (2012), The mechanisms of sea ice melt

pond formation and evolution, *J. Geophys. Res. C (Oceans)*, *117*, C01,001 (23 pp.),

doi:10.1029/2011JC007,231.

Pringle, D. J., J. E. Miner, H. Eicken, and K. M. Golden (2009), Pore-space perco-

lation in sea ice single crystals, *J. Geophys. Res. (Oceans)*, *114*, C12,017, 12 pp.,

doi:10.1029/2008JC005,145.

Reid, J. E., A. Pfaffling, A. P. Worby, and J. R. Bishop (2006), In situ measurements of

the direct-current conductivity of Antarctic sea ice: Implications for airborne electro-

magnetic sounding of sea-ice thickness, *Ann. Glaciol.*, *44*, 217–223.

- 277 Rysgaard, S., R. N. Glud, M. K. Sejr, J. Bendtsen, and P. B. Christensen (2007), Inorganic
278 carbon transport during sea ice growth and decay: A carbon pump in polar seas, *J.*
279 *Geophys. Res.*, *112*, C03,016, doi:10.1029/ 2006JC003,572.
- 280 Rysgaard, S., J. Bendtsen, L. T. Pedersen, H. Ramløv, and R. N. Glud (2009), Increased
281 CO₂ uptake due to sea ice growth and decay in the Nordic Seas, *J. Geophys. Res.*, *114*,
282 C09,011, doi:10.1029/2008JC005,088.
- 283 Sampson, C., K. M. Golden, A. Gully, and A. P. Worby (2011), Surface impedance to-
284 mography for Antarctic sea ice, *Deep Sea Res. II*, *58*, 1149–1157.
- 285 Serreze, M. C., M. M. Holland, and J. Stroeve (2007), Perspectives on the Arctic’s shrink-
286 ing sea-ice cover, *Science*, *315*, 1533–1536.
- 287 Stauffer, D., and A. Aharony (1992), *Introduction to Percolation Theory, Second Edition*,
288 Taylor and Francis Ltd., London.
- 289 Stogryn, A., and G. J. Desargant (1985), The dielectric properties of brine in sea ice at
290 microwave frequencies, *IEEE Trans. Antennas Propagat.*, *AP-33*(5), 523–532.
- 291 Thomas, D. N., and G. S. Dieckmann (Eds.) (2009), *Sea Ice, 2nd Edition*, Wiley-Blackwell,
292 Oxford.
- 293 Thyssen, F., H. Kohnen, M. V. Cowan, and G. W. Timco (1974), DC resistivity measure-
294 ments on the sea ice near pond inlet, *Polarforschung*, *44*, 117–126.
- 295 Wong, P. (1988), The statistical physics of sedimentary rocks, *Physics Today*, *41*(12),
296 24–32.

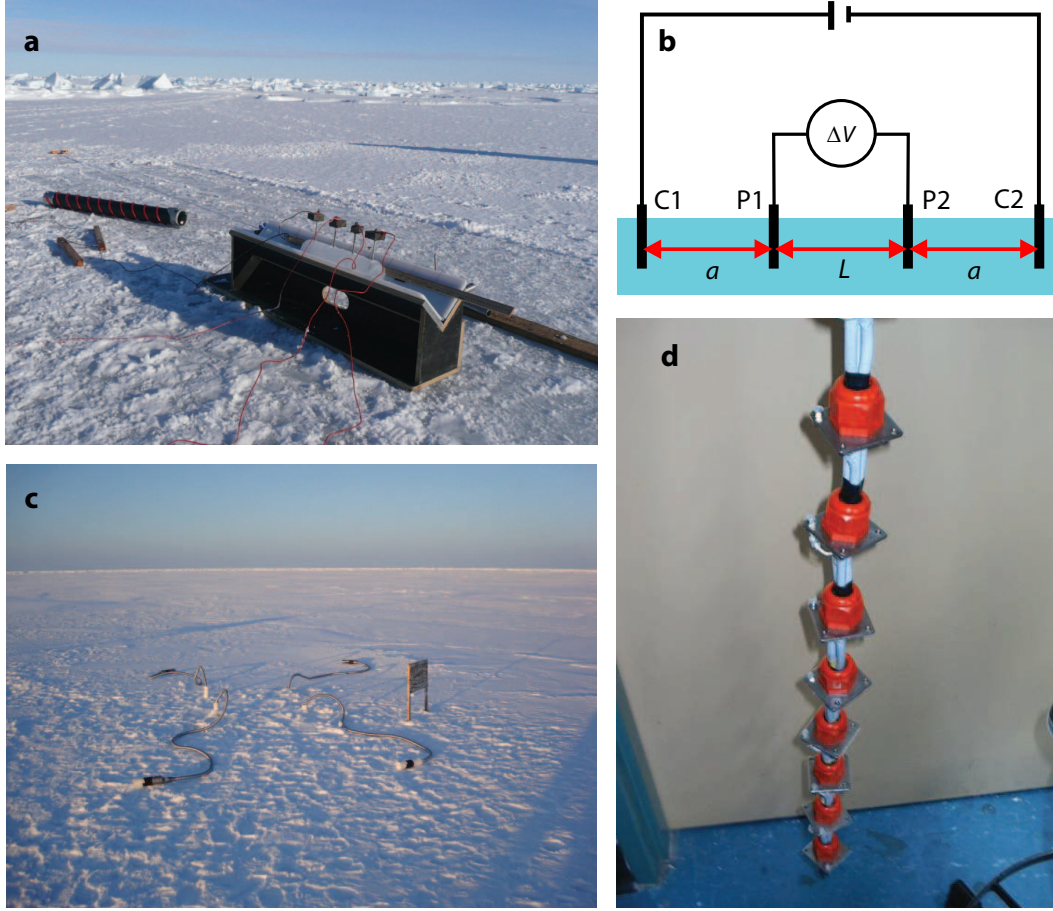


Figure 1. (a) A Wenner electrode array is configured to measure the vertical conductivity of Antarctic sea ice, by inserting the four probes into an extracted ice core. (b) A current I is injected into the core through the outer electrodes C1 and C2. The potential difference ΔV resulting from the current flow is measured by the inner electrodes P1 and P2. The ratio $\Delta V/I$ is the resistance R in ohms. Here the electrode spacing is $L = 10$ cm and $a = 10$ cm. (c) A cross-borehole array is frozen into Arctic sea ice. The DC resistivity profile was tomographically reconstructed in the volume enclosed by the electrode strings. One of the strings, with 10 cm separation of the plates, is shown in (d).

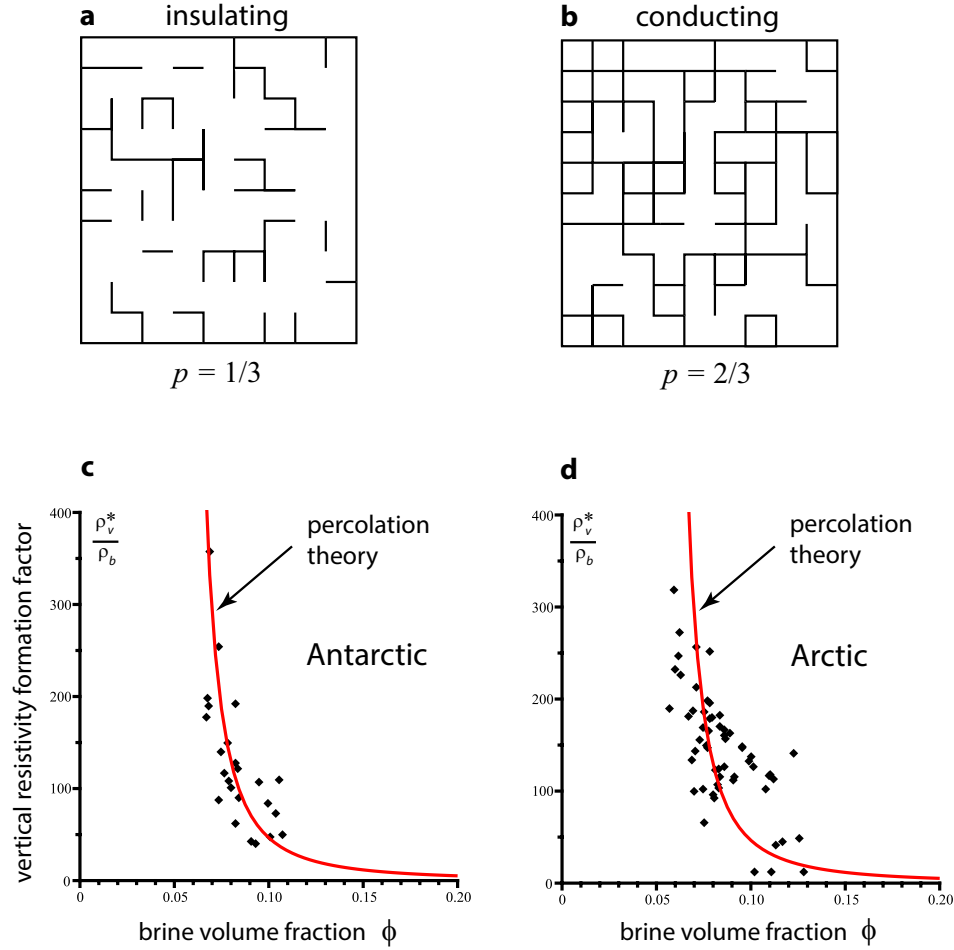


Figure 2. The two dimensional square lattice below its percolation or connectivity threshold $p_c = 1/2$ in (a), and above in (b). We display the vertical resistivity formation factor data from the Antarctic in (c) and the Arctic in (d), along with the same prediction from percolation theory in each. Both data and theory exhibit divergent behavior as ϕ approaches $\phi_c \approx 0.05$ from the right, with a vertical asymptote at $\phi = \phi_c$, electrically signaling the transition to relatively impermeable ice.

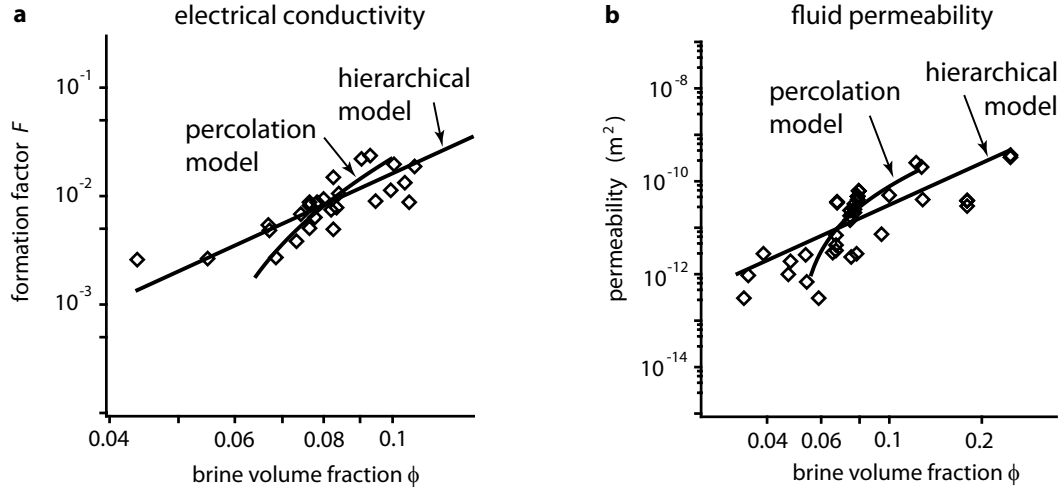


Figure 3. (a) Antarctic field data on the vertical formation factor $F = \sigma_v^*/\sigma_b$ is compared with the hierarchical model $F(\phi) = F_0\phi^3$. The prediction of percolation theory is also shown. (b) Comparison of Arctic fluid permeability data with the hierarchical model, along with percolation theory [Golden *et al.*, 2007]. In both figures percolation theory captures the trend of the data in the percolation regime more closely than Archie’s law.

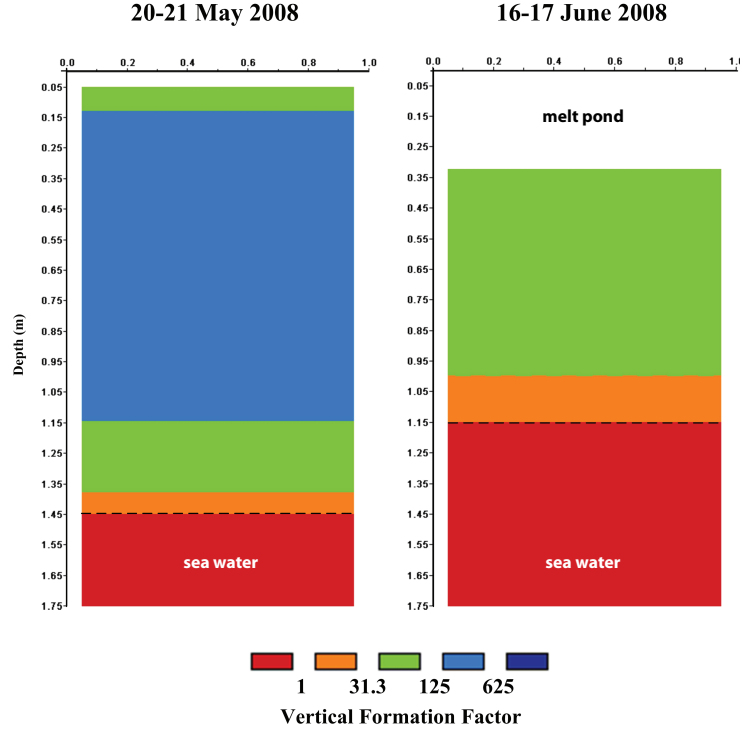


Figure 4. Cross-borehole tomographic reconstructions of the vertical resistivity formation factor for Arctic sea ice before (a) and after (b) melt pond formation. The evolution of resistivity structure is consistent with warming of the ice, thus increasing the fluid permeability and facilitating the infiltration of meltwater into the upper layer of sea ice from the surface. To connect the electrical properties of sea ice to its important processes, the range of the resistivity formation factor G is divided into five regimes: $G > 625$ (ice impermeable enough to allow ponds to grow for surface ablation rates 10 cm/d or larger for a critical pore radius of 0.1 mm); $125 < G \leq 625$, blue (ice impermeable enough to allow ponds to grow for surface ablation rates between 10 and 50 cm/d for a critical pore radius of 0.1 mm); $31.3 < G \leq 125$, green (at formation factors of 31.3 or larger ice is impermeable from the perspective of CO_2 exchange and build-up of nutrients and biomass in the ice [Rysgaard *et al.*, 2007], and sufficiently impermeable to drainage to support surface ponding); $1 < G \leq 31.3$, orange (highly permeable ice that allows for CO_2 pumping and build-up of nutrients and biomass); $G \leq 1$, red (assumed to be free water column). Only the most resistive ice $G > 625$ is not shown.

7. Auxiliary Material: Percolation Theory for Sea Ice

Lattice and continuum percolation theories [Stauffer and Aharony, 1992] have been used to model a broad range of disordered materials where the connectedness of one phase dominates effective transport behavior. Consider the square ($d = 2$) or cubic ($d = 3$) network of bonds joining nearest neighbor sites on the integer lattice \mathbb{Z}^d . The bonds are assigned electrical conductivities $\sigma_0 > 0$ (open) or 0 (closed) with probabilities p and $1 - p$. Groups of connected open bonds are called open clusters, and the average cluster size grows as p increases. In this model there is a critical probability p_c , $0 < p_c < 1$, called the *percolation threshold*, where an infinite cluster of open bonds first appears. In $d = 2$, $p_c = \frac{1}{2}$, and in $d = 3$, $p_c \approx 0.25$. Typical configurations for the $d = 2$ square lattice above and below the threshold are shown in Figure 2 a and b.

Let $\sigma^*(p)$ be the effective conductivity of the network in the vertical direction [Stauffer and Aharony, 1992]. For $p < p_c$, $\sigma^*(p) = 0$. For $p > p_c$ and near p_c , $\sigma^*(p)$ exhibits power law behavior,

$$\sigma^*(p) \sim \sigma_0(p - p_c)^t, \quad p \rightarrow p_c^+, \quad (3)$$

where t is the conductivity critical exponent. For lattices, t is believed to be universal, depending only on d . In $d = 2$, $t \approx 1.3$, and in $d = 3$, $t \approx 2.0$ [Stauffer and Aharony, 1992]. There is also a rigorous bound [Golden, 1990] that $1 \leq t \leq 2$ in $d = 2$ and $d = 3$. Since $\sigma^*(p) \rightarrow 0$ as $p \rightarrow p_c^+$, the effective resistivity $\rho^*(p) = 1/\sigma^*(p)$ diverges as $p \rightarrow p_c^+$, with a vertical asymptote at $p = p_c$. For two phase composites with finite component resistivities, like sea ice, the behavior only approximates the asymptote, and for $p < p_c$, ρ^* remains finite.

The fluid permeability $\kappa^*(p)$ corresponding to (1), where the open bonds are pipes of fluid conductivity $\kappa_0/\eta = r_0^2/8\eta$ and radius r_0 , behaves like $\kappa^*(p) \sim \kappa_0(p - p_c)^e$ as $p \rightarrow p_c^+$, with e

the fluid permeability exponent and η the fluid viscosity. For lattices, it is believed [Stauffer
and Aharony, 1992] that $e = t$. In the continuum, the exponents e and t can take non-universal
values, and need not be equal, such as for the three dimensional Swiss cheese model [Halperin
et al., 1985; Stauffer and Aharony, 1992]. However, for lognormally distributed inclusions, as in
sea ice, the behavior is *universal* [Golden et al., 2007; Berkowitz and Balberg, 1992]. Thus for sea
ice, $t = e \approx 2$.

In order to use percolation theory to quantitatively describe the vertical conductivity $\sigma_v^*(\phi)$,
and to provide a link between fluid and electrical transport in sea ice, we recall our result [Golden
et al., 2007] for the vertical fluid permeability

$$k_v^*(\phi) \sim 3 (\phi - \phi_c)^2 \times 10^{-8} \text{ m}^2, \quad \phi \rightarrow \phi_c^+. \quad (4)$$

The scaling factor $k_0 = 3 \times 10^{-8}$ is estimated using critical path analysis [Stauffer and Aharony,
1992; Friedman and Seaton, 1998]. The effective behavior of media with a broad range of local
conductances is dominated by a critical *bottleneck* conductance related to the minimal radius in
a connected pathway of appropriate scale. To relate σ_v^* to k_v^* , we use the following relation from
critical path analysis [Friedman and Seaton, 1998]. With r_c denoting the critical radius for our
centimeter scale electrical experiments, then

$$k_v^* = \frac{r_c^2}{8} \frac{\sigma_v^*}{\sigma_b}, \quad (5)$$

where σ_b is the conductivity of brine, which depends [Stogryn and Desargant, 1985] on tempera-
ture T . By measuring the radii of vertical pathways in X-ray tomography images [Golden et al.,
2007; Pringle et al., 2009], we estimate a range in mm of $0.1 \leq r_c \leq 0.2$.

It is useful to consider the vertical conductivity formation factor $F = \sigma_v^*/\sigma_b$, which removes the
dependence of the effective parameter on the changing conductivity of the brine, and depends

only on the pore volume fraction and geometry. In view of (1) and (??), $F(\phi) \sim F_0 (\phi - \phi_c)^2$ as $\phi \rightarrow \phi_c^+$, where $F_0 = 8k_0/r_c^2$. The estimates of 0.1 mm to 0.2 mm for r_c yield a range for F_0 of $6 \leq F_0 \leq 24$.

In order to compare our conductivity measurements with percolation theory, we must exclude data below $\phi_c \approx 0.05$ [Golden *et al.*, 2007], since the theory is only valid for $\phi > \phi_c$. It is more illustrative to display the data in terms of the reciprocal $G = 1/F = \rho_v^*/\rho_b$, which is the vertical resistivity formation factor. In Figure 2 c and d we show the two data sets from the Antarctic and Arctic. By fixing the exponent $t = 2$ and the threshold value $\phi_c = 0.05$ in the above expression for $F(\phi)$, a statistical best fit of the data yields a value of $F_0 \approx 9$, which lies inside our predicted range, so that

$$F(\phi) \sim 9 (\phi - 0.05)^2, \quad \phi \rightarrow \phi_c^+. \quad (6)$$

We see that the data agree well with the theory, and that they both exhibit divergent behavior with a vertical asymptote at the percolation threshold. Moreover, in the variables $x = \log(\phi - 0.05)$ and $y = \log F$, the line predicted by percolation theory in (??) is $y = 2x + \log F_0$, with $\log F_0 = 0.95$, $F_0 = 9$. Critical path analysis yields the bounds $0.8 \leq \log F_0 \leq 1.4$, and the best fit for the Antarctic data in f is $y = 1.99x + 0.93$, where 0.93 lies inside these bounds. In logarithmic variables, the error of the regression is 0.38 for the Arctic data and 0.22 for the Antarctic data (that is, approximately 68% of the Antarctic data is within 0.22 of the regression line). The increased scatter in the Arctic data is not surprising given the inverse computation required to obtain the formation factor data.

To model $\sigma_v^*(\phi)$ over all porosities, we consider features of the brine phase present over the full range — some degree of small-scale connectivity, and self-similarity. Hierarchical models

of spheres or other grains surrounded by smaller spheres, and so on, with brine in the pore spaces [Golden *et al.*, 2007], were used to model $k_v^*(\phi)$. The simplest model yields a result of $k_v^*(\phi) = k_0 \phi^3$. Via (??) we obtain an Archie's law result of $F(\phi) = F_0 \phi^3$. A statistical best fit of our Antarctic data yields a value of $F_0 \approx 16$, which is in the estimated range. In Figure 3 a, our Antarctic data is shown along with fits derived from both models, and in b, Arctic permeability data [Golden *et al.*, 2007] is shown relative to predictions from both models.

Plate electrodes in contact with the ends of a cylinder generate parallel field lines which make measuring the conductivity of the cylinder material relatively straightforward, as illustrated in Figure 5 a. To assess the accuracy of our four probe method, the commercial package Comsol 3.5a was used to create a finite element model of cylindrical sea ice cores 0.09 m in diameter and 0.5 m in length. Four metal probes of 0.004 m in diameter and 0.09 m in length were inserted approximately 0.07 m into the core, similar to Figure 1 b. When the current is injected through the outer probes instead of parallel plates, as in Figure 5 b, the nearby field lines show significant curvature. However, in the boxed measurement region in Figure 5 b where the inner probes are located, the field lines are relatively straight, thus minimizing the error between the actual conductivity of the material and what is measured by the array. Numerical simulations show that if the outer probes are 5 cm or more from the inner measurement region, this error is less than 8.5%, and is less than 1.5% if the distance is 10 cm or more, as for much of our data.

When extracting a sea ice core to measure its properties, loss of brine is a principal concern. However, for our experiments we did not see any evidence of significant brine loss during the relatively short measurement periods with air temperatures ranging from about -6°C to -18°C (with most below -9°C). Moreover, the probes are inserted deep into the core, minimizing

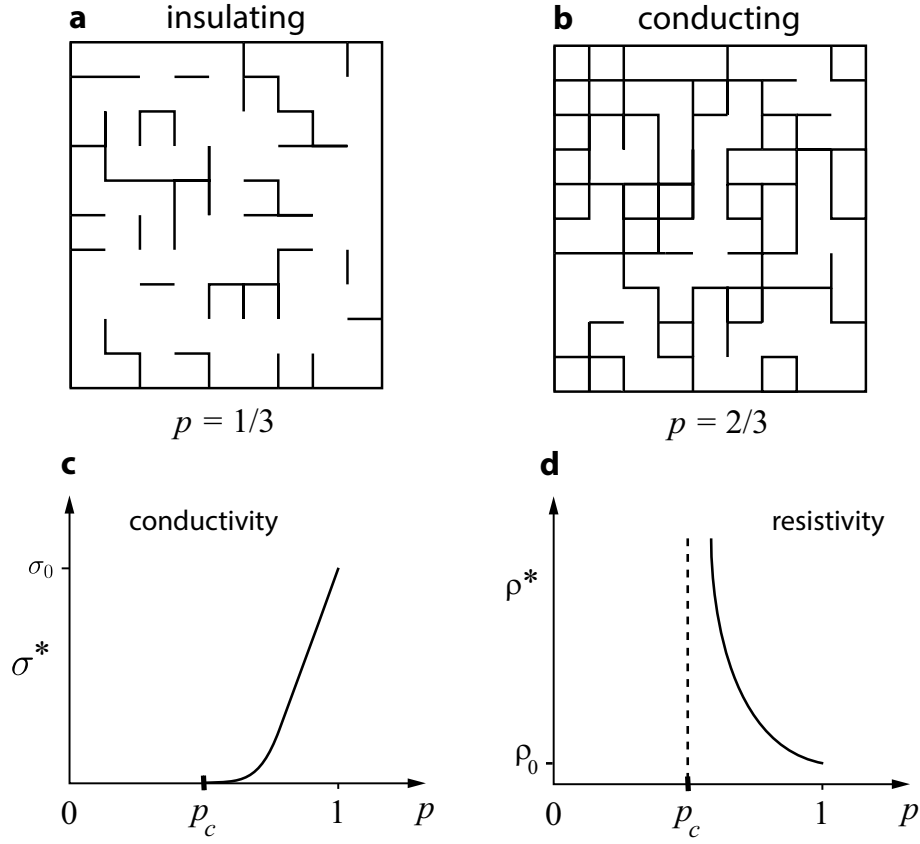


Figure 5. The two dimensional square bond lattice below its percolation or connectivity threshold $p_c = 1/2$ in (a), and above in (b). Below p_c , there is no bulk transport, and above p_c the effective conductivity takes off with power law behavior, as shown in (c). In (d) the effective resistivity diverges as p approaches p_c from the right, with a vertical asymptote at $p = p_c$.

contact with potential brine surface films. Our numerical simulations and these observations establish the Wenner array as a viable field method for *direct* resistivity measurements.

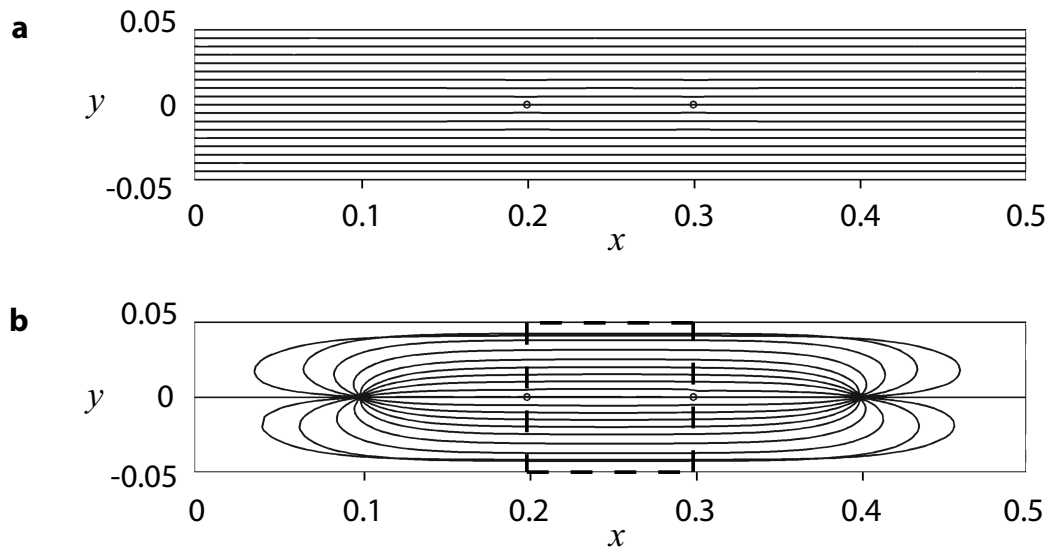


Figure 6. Comparison of field lines for a parallel plate configuration in (a) with those for a four probe Wenner array in (b).